

Numerical and experimental study of mechanical behaviors of the steel-confined rubber bearing



Di Wu ^{a,c}, Yan Xiong ^b, Zhenyu Yang ^{a,c,*}

^a Key Laboratory of Earthquake Engineering and Applied Technique of Guangdong Province, Guangzhou University, Guangzhou 510405, China

^b State Key Laboratory of Subtropical Building Science, South China University of Technology, Guangzhou 510640, China

^c Earthquake Engineering Research and Test Center, Guangzhou University, Guangzhou 510405, China

ARTICLE INFO

Keywords:

Steel-confined
Three-dimensional seismic isolation
Isolator
Rubber bearing
Quasi-static test

ABSTRACT

The conventional laminated rubber bearing is primarily for the horizontal seismic input. To achieve three-dimensional seismic isolation, the horizontal laminated steel plates in rubber bearings are replaced by externally confined steel plates, which is the steel-confined rubber bearing (SCRB). The external steel cover effectively increases the stability of the rubber bearing, while acting as a U-shaped steel cover and improving the energy dissipation capacity of the isolator. The mechanical properties of the SCRBs were investigated based on finite element analysis and experiments. The test and numerical results show that the SCRB has a low horizontal and vertical stiffness, while the external steel cover provides additional damping for the rubber isolator. The modified Bouc-Wen model was introduced to simulate the horizontal and vertical force-displacement hysteresis relationship of the SCRB. Based on FE model simulations, the effects of area coverage, quantity and length of steel cover on vertical stiffness, horizontal stiffness and equivalent damping ratio of the SCRB were analyzed in detail. A design procedure of the SCRB based on the stiffness is proposed. Finally, the effectiveness of the SCRB on reducing horizontal and vertical seismic responses is validated using a single-degree-of-freedom system.

1. Introduction

Seismic isolation is recognized as an effective way to improve the seismic performance of buildings and bridges [1]. Laminated rubber bearings, which have high vertical loading capacity and small horizontal stiffness with high damping, are widely used in seismic isolation for engineering structures. Past earthquakes have validated the effectiveness of horizontal seismic isolators, including rubber bearings for buildings [2,3] and bridges [4].

Despite the widely-used horizontal isolation, some certain engineering structures, including long-span structures, electronic equipment and buildings on metro lines, still need to face the problem of vertical vibration or seismic inputs. For example, the transformer has sidewall bushings inclined installed, so vertical seismic isolation is needed [5]. Recently, several horizontal isolators, remaining a large vertical stiffness, have been developed [6,7]. In non-seismic areas, the vertical vibration on buildings can be reduced by disc springs [8] and geosynthetics isolators [9], which have small vertical stiffness and large loading capacity. However, in seismic areas, conventional popular seismic isolators, including laminated rubber bearings and friction

pendulum isolators, exhibit large stiffness in the vertical direction. Meanwhile, a parametric analysis shows that the acceptable period of the vertically isolated buildings ranges from 0.5 to 1.0 s [10,11]. As a result, thick rubber bearings, which reduce the vertical stiffness by increasing the thickness of rubber in each layer, are proposed [12]. The test results show that a shape factor decreased from 16.7 to 4.0 in rubber bearings successfully reduces the vertical stiffness from 500 kN/mm to only 50 kN/mm [13], but the conventional seismic isolators cannot achieve such flexibility in the vertical direction. A shaking table test shows that thick high damping rubber bearings, with vertical stiffness around 500 kN/mm, can effectively reduce the metro-induced vertical high-frequency vibrations [14]. The field measurements also validate that a thick rubber bearing, with vertical stiffness of only 24 kN/mm, can reduce the vertical acceleration of a two-story building by 28 dB [15]. However, the increase in the thickness of the rubber layer in the bearing will lead to a decrease in the stability of the bearing, which will reduce the vertical bearing capacity of the bearing.

The disk springs, which are widely used as vertical isolators in industrial sectors, are installed on rubber bearings to form the three-dimensional seismic isolation [16]. Similarly, hydraulic cylinders [17],

* Corresponding author.

E-mail address: yang_zy@gzhu.edu.cn (Z. Yang).

air springs [18,19], and high damping rubber [20] installed on conventional rubber bearings provide considerable vertical isolation effects. Alternatively, the vertical isolators can also be installed on friction pendulum sliders [21,22]. Since the laminated rubber bearings have an excellent isolation effect in the horizontal direction, the assembled three-dimensional isolation consisting of inclined rubber bearings is proposed [23]. A numerical analysis shows that an assembled isolation using three inclined rubber bearings and a horizontal one can reduce the vertical acceleration response by 33% [24]. Alternatively, the vertical vibration damping can also contribute from the foundation, for example, the rubber under-ballast mat [25], sometimes made of recycled elastomers [26]. Similarly, the vertical vibration of machines can be reduced using an underground rubber sheet [27].

Generally, the rubber bearings should be tested to obtain the mechanical properties and hysteresis behaviors under cyclic loads [28]. In addition, the theoretical analysis [29], as well as the finite element (FE) model [30], can also predict the behaviors of rubber bearings. The test results show that the FE analysis can accurately simulate the hysteresis curves of rubber bearings under compression and shear forces [31,32,33]. Therefore, based on existing methods for modeling rubber materials, the FE analysis is adopted in the development of innovative rubber bearings with other reinforcements, including shape memory alloys[34], yielding shear devices[35], and steel rings[36].

For three-dimensional seismic isolation, the rubber bearing pursues high vertical bearing capacity, as well as low horizontal and vertical stiffness. Moreover, the bearing still needs a simple and reliable structure to be acceptable and feasible in engineering practice. In this manuscript, FE analysis and experimental studies are carried out for the proposed steel-confined rubber bearing (SCRB) [37] to reveal its mechanical properties in horizontal and vertical directions. First, the components and construction of the proposed SCRB have been analyzed. Then, the bearing specimens were tested by quasi-static compression and compression-shear tests to verify the reliability of the numerical analysis results. Further, a FE analysis of the bearing is conducted to investigate the three-dimensional mechanical behavior of the bearing and the design procedure of the SCRB is proposed. Finally, the effectiveness of the SCRB on reducing seismic responses is validated.

2. Components and experiments of the SCRB

2.1. Components and configuration of the SCRB

The conventional steel-laminated rubber bearing constrains the horizontal deformation of the rubber block by inter-layer steel plates. Meanwhile, the SCRB in this study cancels the inter-layer steel plates and restricts the deformation of the rubber block by U-shaped steel plates outside the rubber block, and the specific components and configurations are shown in Fig. 1. A drum-type rubber block (DRB) is used to match the shape of the U-shaped steel covers. The U-shaped steel covers can serve as the stiffeners of the rubber material, as well as energy dissipation components.

Fig. 2 shows the typical installation of the SCRB on columns of a building. If the SCRB has a smaller diameter than the column, the SCRB can be installed like a conventional laminated rubber bearing. Since the SCRB is quite flexible vertically, so the diameter of the SCRB potentially is larger than that of the column. If the SCRB has a large diameter, the column needs to be enlarged near the SCRB.

2.2. Specimen and test configuration

To investigate the actual mechanical behaviors of the SCRB, a specimen was constructed and tested. Fig. 3 shows the specimen and the dimension parameters, while Fig. 4 shows the test facility. An SCRB specimen was tested to validate the effectiveness of steel covers and the correctness of the numerical analysis. The steel covers were made into U-shape ones, then connected to end plates of the drum-type rubber bearing by 16 M20 bolts. To provide space for the bolts, there were two end plates embedded in the drum-type rubber. The inner end plates will reduce the effective thickness of the rubber. In the specimen, the actual thickness of the rubber was 57 mm, smaller than the height of 97 mm of the SCRB. In addition, two load plates were introduced to provide flat planes for the test facility. In addition, two hold devices were added to prevent the transfer of horizontal shear forces from load plates to the specimen.

The temperature in the laboratory was 23°C. The specimen was installed on the load-shear test machine, which can apply vertical and horizontal forces on the bearing at the same time. The reaction force and the horizontal displacement were recorded by the built-in program of the test facility. Additionally, three displacement sensors were used to

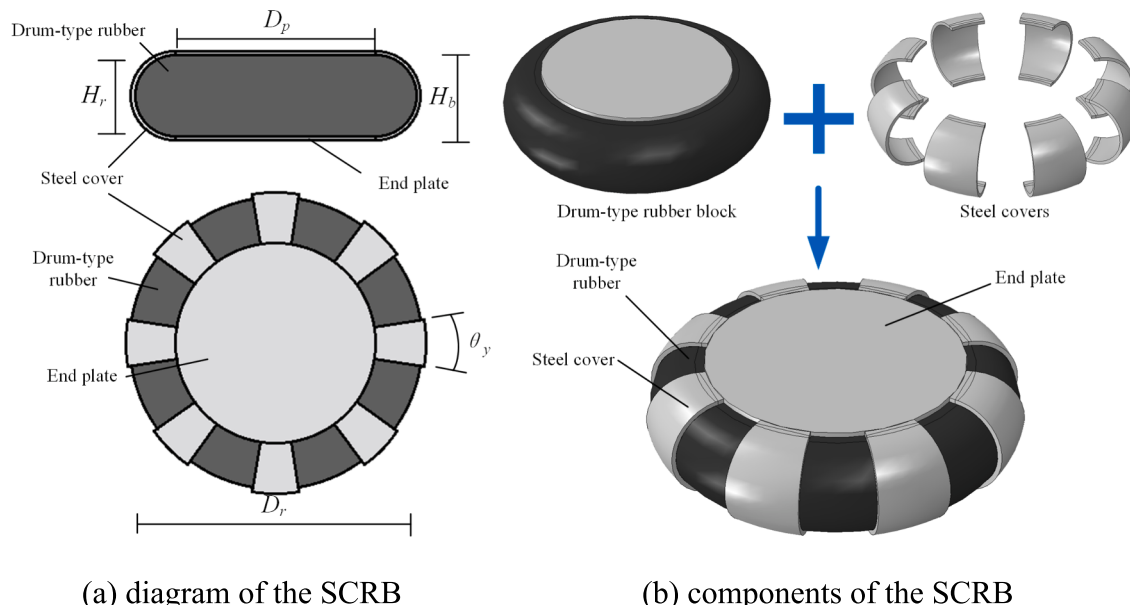


Fig. 1. Components and diagram of the steel-confined rubber bearing.

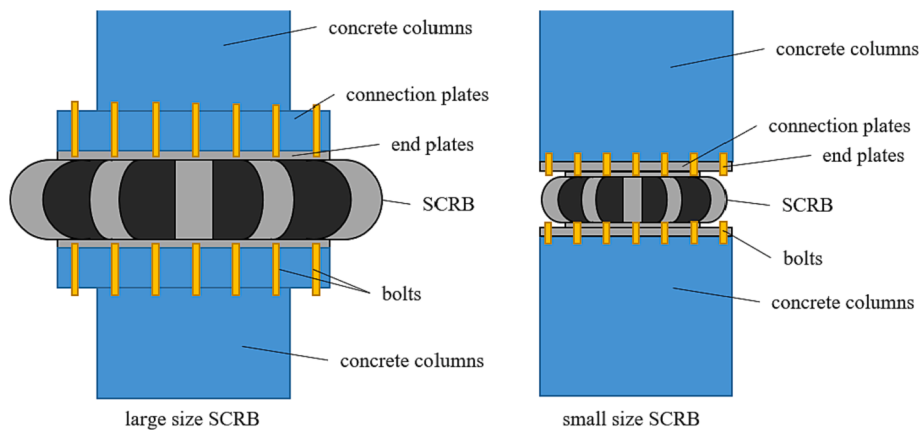


Fig. 2. Typical installations of the SCRB on columns of buildings.

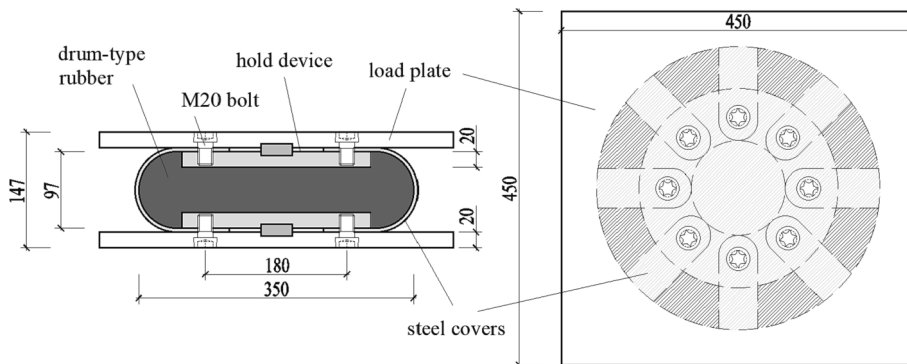


Fig. 3. Components and diagram of the SCRB specimen.

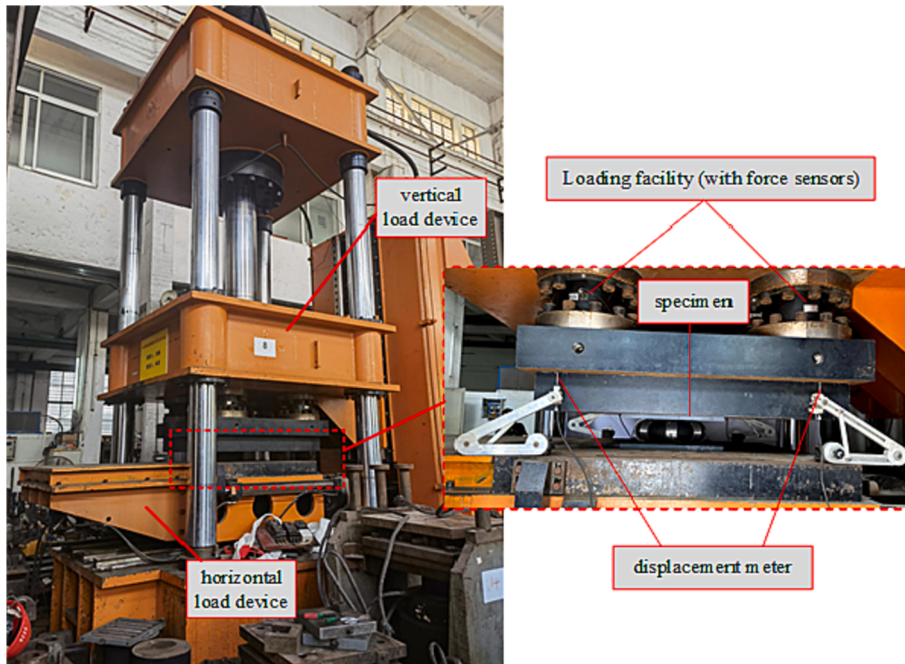


Fig. 4. The test facility for the SCRB specimen.

obtain the vertical deformation of the specimen, as there might be ununiform deformation. The test scenarios are listed in Table 1.

In the vertical test, the specimen was subject to design load P_0 of 122.66 and 245.31 kN, which are equal to pressure loads of 2.5 and 5.0

MPa, respectively, as shown in Fig. 5. The loading curves in C25 and C50 programs are plotted in Fig. 4(a). As specified in the code [38], P_1 and P_2 , the lower and upper limits, are 0.7 P_0 and 1.3 P_0 , respectively.

Then, the specimen was subject to horizontal cyclic loads with a

Table 1
Scenarios of the test.

Scenario	Vertical pressure (MPa)	Shear strain
C25	2.5	0
C50	5.0	0
S25	2.5	50%
S50	5.0	50%

constant vertical load in S25 and S50 scenarios. In the horizontal test, the specimen was loaded at specified horizontal displacement, peaking at 30 mm. The test was loaded with a sine curve at a frequency of 0.05 Hz, and the loading curve is shown in Fig. 4(b).

2.3. Test results

The specimen was first loaded in the vertical direction. As shown in Fig. 6, the SCRB generated significant horizontal deformation under the vertical loads. In the C25 scenario, the steel covers and the drum-type rubber both deformed slightly. Then, when the vertical load increased, as predicted by the numerical results, the drum-type rubber block generated significant horizontal deformation, the width of the specimen enlarged and the drum-type rubber contacted the load plates. Meanwhile, the steel covers, as well as the load plates, limit the deformation of the rubber block.

Fig. 7 shows the reaction forces and corresponding deformation of the specimen under cyclic vertical loads. The vertical stiffness is estimated using the cyclic segment of the test result, according to the Chinese code [38]. In the C25 scenario, the SCRB shows approximately linear behaviors in the loading procedure with a stiffness of about 24.73 kN/mm when the specimen experiences cyclic loads. Similarly, the vertical stiffness of the SCRB in the C50 scenario is 34.38 kN/mm in the cyclic stage.

Compared with other innovative rubber bearings in other studies, the SCRB has a much smaller vertical stiffness when they have a similar diameter. For example, the polyurethane elastomeric bearing [6] has a vertical stiffness of 1600kN/mm, and the fiber bearing [39] has a vertical stiffness up to 5000 kN/mm. According to previous studies, the bearing with a vertical stiffness between 500 and 25 kN/mm [14,15] has a considerable effect in reducing the vertical response, and the SCRB meets this requirement.

After the vertical load procedure, the SCRB specimen was subject to cyclic horizontal motions up to 30 mm, with a vertical preload of 122.66 and 245.31 kN, respectively. As shown in Fig. 8, the specimen, including the rubber part and the steel covers, generates significant deformation.

Fig. 9 shows the hysteresis curves of the SCRB specimen in the two tests. As the rubber can contact the load plates during the test, and the friction coefficient between the rubber and steel material reaches 0.85, the friction between the SCRB and the load plates should be considered in the numerical analysis. With the increase in the vertical preload, the

equivalent horizontal stiffness of the specimen only slightly increases from 1.61 kN/mm to 1.87 kN/mm, while the equivalent damping ratio keeps nearly unchanged. Besides, the numerical analysis can effectively predict the horizontal behaviors of the SCRB.

2.4. The practical constitutional model of the SCRB

Although a detailed FE model can predict the structural behaviors of the SCRB, it is quite hard to include such a fine FE model in the seismic analysis of buildings. Therefore, a simplified macro model for the SCRB is needed.

In the horizontal direction, the hysteresis curves of the SCRB are similar to those of lead rubber bearings, so the Bouc-Wen model can be used:

$$F(t) = \alpha k_u u(t) + (1 - \alpha) k_z z(t) \quad (1)$$

where $F(t)$ is the reaction force, $u(t)$ is the deformation, and $z(t)$ is the hysteretic variable, which can be expressed as:

$$z = \{A - [\beta \text{sign}(z \cdot \dot{u}) + \gamma] \cdot |z|^n\} \dot{u} \quad (2)$$

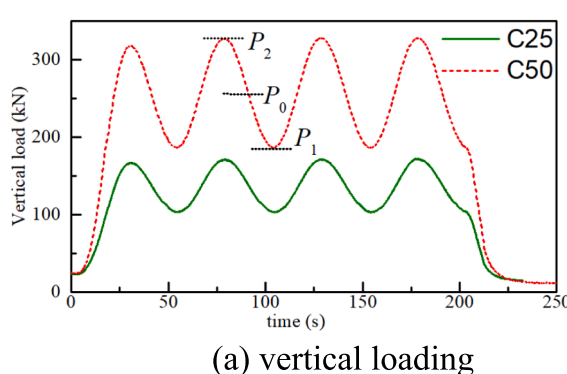


(a) SCRB in the C25 scenario

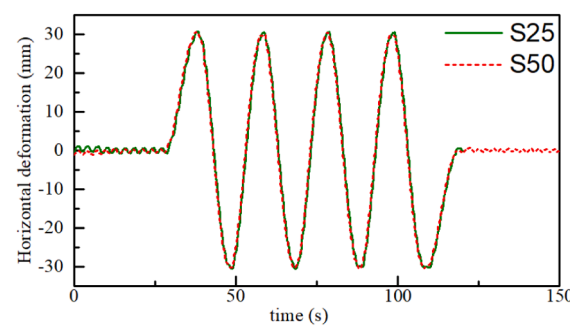


(b) SCRB in the C50 scenario

Fig. 6. Deformation of SCRB under the vertical loading.



(a) vertical loading



(b) horizontal loading

Fig. 5. Loading time history of various scenarios.

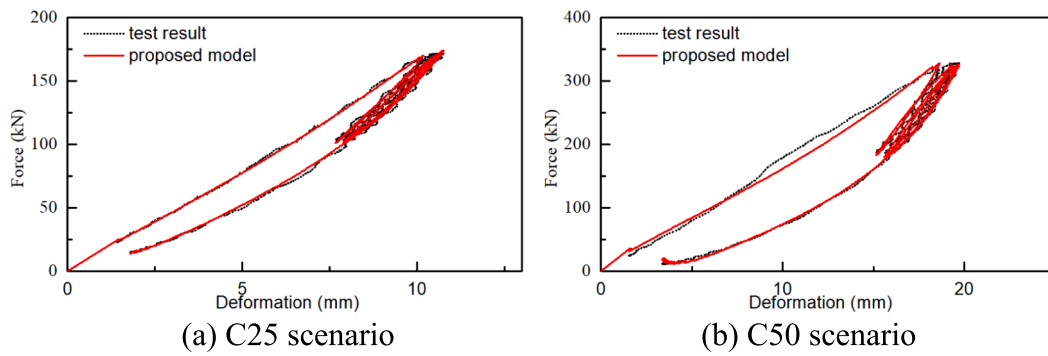


Fig. 7. Reproduction of force–deformation curves of the SCRB in the horizontal direction.



(a) S25 scenario



(b) S50 scenario

Fig. 8. Deformation of the SCRB under horizontal motions

where A , β , γ , and n are hysteresis parameters. By fitting the test data, the parameters of the Bouc-wen model are identified, as listed in Table 2. The fitting of parameters is conducted using the built-in least square function “leastsq” in Python. As shown in Fig. 7, the Bouc-Wen model can accurately reproduce the horizontal hysteresis curves of the SCRB.

In the vertical direction, as predicted in Fig. 7, the SCRB exhibits hardening in compression and softening in tension. Therefore, the modified Bouc-Wen model [40,41] is employed, and Equation (1) is rewritten as:

$$F(t) = k_e(\exp(b_1 u(t)) + \exp(-b_2 u(t))) + k_i z(t) \exp(\alpha u(t)) \quad (3)$$

where b_1 , b_2 , and k_e are introduced to describe the varying stiffness. Using the parameters listed in Table 2, the vertical force-deformation curves of the SCRB can be accurately reproduced, as shown in Fig. 9. The modified Bouc-Wen model can be used to describe the vertical behaviors of the SCRB.

3. Mechanical behaviors of the SCRB with various parameters: The numerical approach

3.1. FE modeling of the SCRB

The FE model of the bearing was developed using ABAQUS. The values of the parameters of the prototype SCRB are listed in Table 3. The rubber has an international rubber hardness degree (IRHD) of 50, so the elastic and shear module are 2.2 and 0.64 MPa, respectively. To investigate the influence of the parameters on the mechanical behavior of the SCRB, some parameters vary in specified ranges. The first line of the value of the variable parameter is the default one, while the range in the blanket refers to the varying ranges. Fig. 10 shows the SCRB with various configurations.

The bearing was modeled using solid elements, including the rubber bearing and steel plates. The rubber part of the bearing was modeled using the C3D8RH element, which was widely used for hyperelastic materials. The strain energy potential employed the Neo Hooke model. The Neo Hooke coefficients in hyperplastic material, C_{10} was 0.32, which was derived from the shear module of rubber material with hardness 50, while D_1 was 0.002 to consider the slight compressibility of

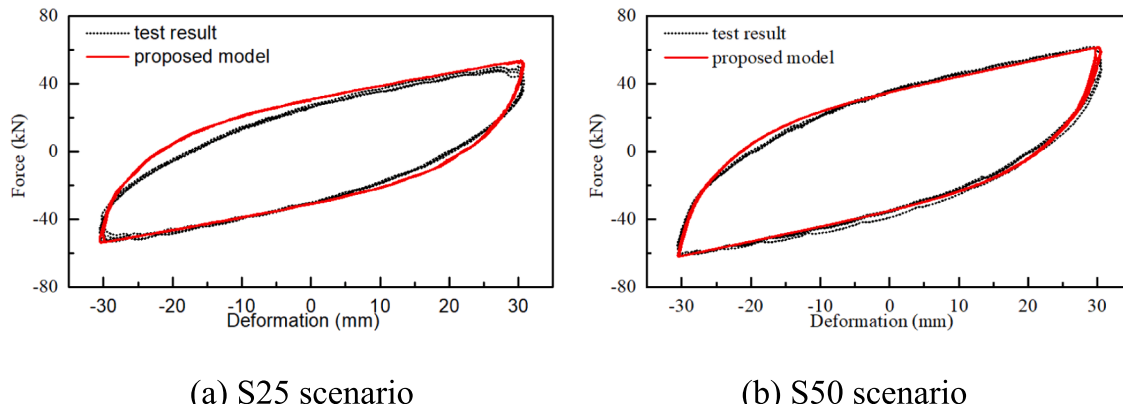


Fig. 9. Reproduction of hysteresis curves of the SCRB in the horizontal direction.

Table 2

Parameters of the proposed Bouc-Wen model for the SCRB.

Scenario	A	β	γ	n	α	k_i	k_e	b_1	b_1
S25	0.25	0.25	-0.125	1.0	0.045	16.4	-	-	-
S50	0.25	0.25	-0.125	1.0	0.045	18.9	-	-	-
C25	0.217	0.134	0.366	1.0	0.080	21.7	101	0.0756	0.0391
C50	0.344	0.130	0.246	1.0	0.0368	34.4	627	0.0314	-0.0167

Table 3

The values of parameters in the bearing.

Parameter	Description	Value	Parameter	Description	Value
E_0 (MPa)	Elastic module of rubber	2.20	H_b (mm)	Height of the bearing	110
G (MPa)	Shear module of rubber	0.64	H_r (mm)	Height of rubber block	100
D_r (mm)	Outer diameter	430	t_f (mm)	Thickness of end plates	5
D_p (mm)	Diameter of steel plates	280	θ_y (°)	Width of steel covers	18
S_c (%)	Percentage of surface covered	50	t_y (mm)	Thickness of steel cover	5
N_s	Number of steel covers	8			

the rubber material. Meanwhile, C3D8R was used to model the steel part of the bearing. The outer steel covers and endplates were made of Q335 GB/T steel. The constitutional law of the steel was the elastic-perfectly plastic model, while the yield strength was set at 335 MPa. Fig. 11 shows the material and meshing of the FE model of the proposed bearing. The steel covers were intended to be installed on the endplates using bolts.

The steel covers are pressed on the drum-type rubber when the SCRB is subjected to vertical loads. Since the friction coefficient between the

steel and rubber material is as large as 0.85, there is no sliding between the two materials according to preliminary analysis. Therefore, to speed the analysis, the surface of the drum-type rubber is tied with the steel covers.

In engineering practices, the bearing may be installed led under columns that have similar profiles as that of the bearing, so the bottom endplate is fixed. In addition, the vertical and horizontal load were applied via a referring point coupled with the top endplate. A coupling interaction was established between the referring point and the top endplate. As a result, when the vertical load F_v and horizontal load F_h are applied uniformly on the top plate, the top plate only generates translational motions in the vertical and horizontal directions, which is in accordance with the bearing already installed under buildings.

With the FE modeling method, the FE model of the test specimen was established, and loaded using the test data. Figs. 12 and 13 shows the comparison between the numerical and test results. The FE model can predict the mechanical behaviors of the SCRB in both the vertical and horizontal directions.

3.2. Vertical behaviors

In conventional steel-laminated rubber bearings, thin steel plates are inserted in the rubber block to improve the vertical loading capacity of the bearing. Alternately, the proposed SBR employs external steel covers to share the vertical load, and more importantly, prevent the lateral

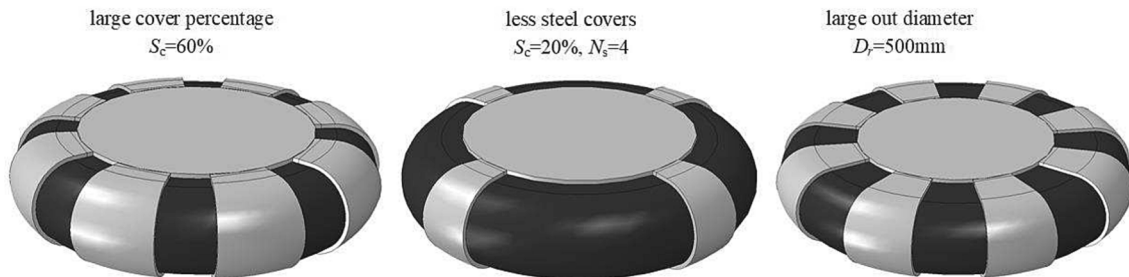


Fig. 10. The appearance of the SCRB with various configurations.

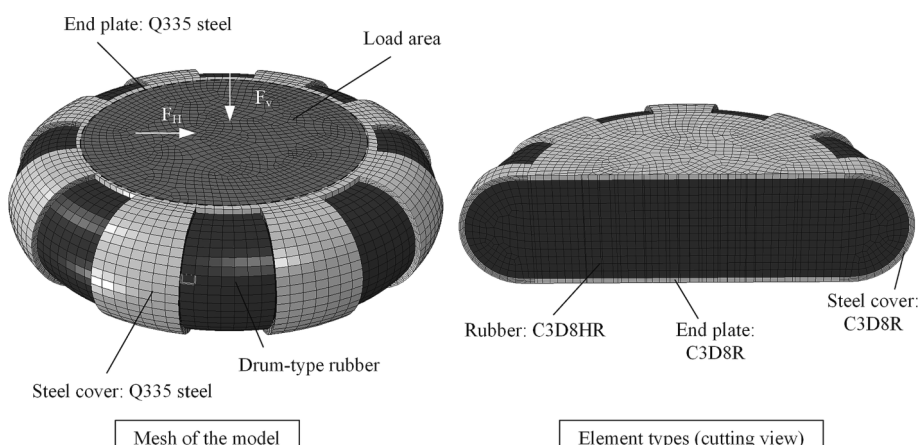
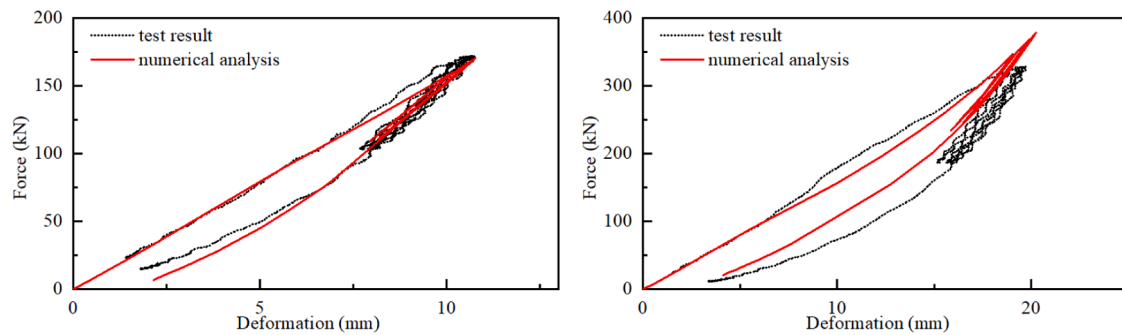


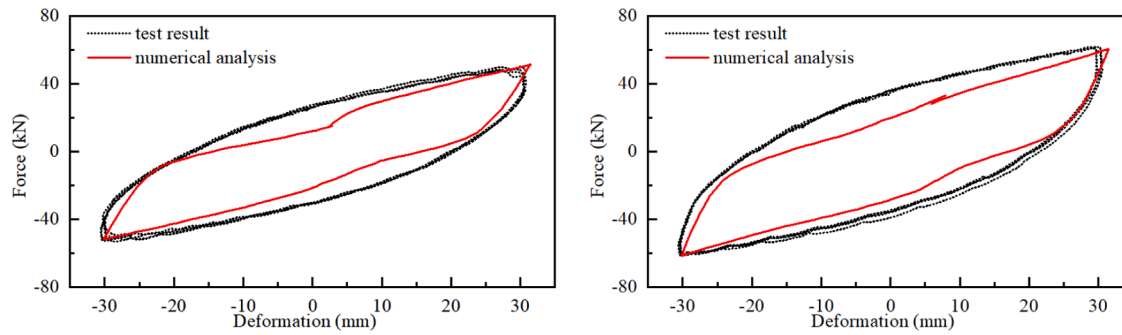
Fig. 11. FE model of the rubber bearings.



(a) C25 scenario

(b) C50 scenario

Fig. 12. Force-deformation curves of the SCRB under vertical loads.



(a) S25 scenario

(b) S50 scenario

Fig. 13. Hysteresis curves of the SCRB under horizontal motions.

deformation of the rubber block. A vertical load F_v was applied to the reference point to obtain the deformation of the bearing.

Fig. 14 shows the effects of the constrain by the steel covers. The DRB and steel covers generate small vertical reaction forces under specified deformation. Meanwhile, the SCRB generates much larger forces, approximately twice the sum of that of the DRB and steel covers. The gray area in **Fig. 14** is the rise in the reaction force contributing from the constraining effect, revealing the effectiveness of the external steel covers.

The rubber part of the SCRB is partially covered by U-steel covers, so the expansion of the rubber concentrates on the uncovered areas. As shown in Fig. 15, when the SCRB is subject to a vertical load up to 330kN, the rubber bulges at uncovered areas between steel covers.

Besides, the maximum nominal strain occurs at the bulge of the rubber part. The U-steel covers experience plasticity under the large vertical load, the plasticity first occurs at the midspan of the steel cover, then expands to terminals.

Since the steel covers significantly affect vertical behaviors of the SCRB, the influence of properties and configuration changes in steel covers are investigated. When the area covered by the steel covers increases from 20% to 70%, the vertical stiffness increases accordingly, as shown in Fig. 16(a). The analysis ends when the maximum shear strain of the rubber part reaches 100%. As the bulging part of the rubber generates the maximum tensile strain, and larger cover percentage results in a smaller strain response under the vertical load. In other words, the increase in the cover percentage increases the reaction force of the SCRB. The SCRB has 8 steel covers in the default configuration, meanwhile, when the cover percentage keeps at 50%, the variation in the number of steel covers has little effect on the vertical stiffness of the SCR, as shown in Fig. 16(b). However, the 9 steel covers configuration ($N_s = 9$), which results in a smaller bulge of the rubber, helps to reduce the maximum tensile strain in the rubber. Therefore, when the cover percentage is specified, long-strip steel covers are recommended.

The shape of steel covers determines the energy dissipation capacity and stiffness, as the D_p keeps at 280 mm, when D_r keeps increasing, the steel cover becomes U-shaped steel, instead of the C-shaped ones when D_r is small. As a result, the vertical stiffness of steel covers decreases. As shown in Fig. 17, when D_r is within 460 mm, 1.62 times D_p , the increase in D_r has little effect on the vertical stiffness. Meanwhile, as D_r exceeds 500 mm, the vertical stiffness of the SCRB decreases considerably. In addition, a larger D_r has little effect on the maximum tensile strain of the rubber, so D_r can be increased when a small vertical stiffness is pursued.

In addition to the increase in vertical stiffness, the supplementary

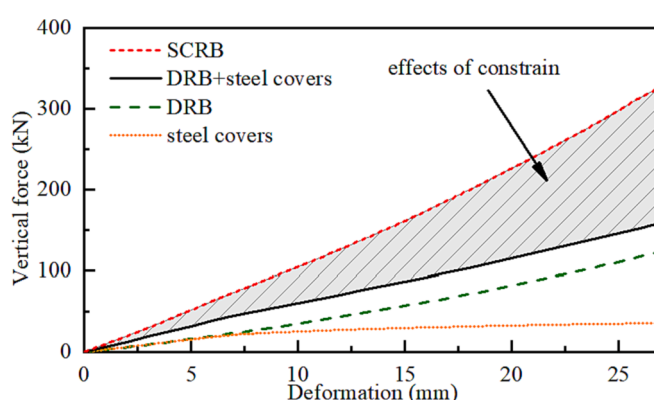


Fig. 14. The reaction forces of SCRB, DRB and external steel covers.

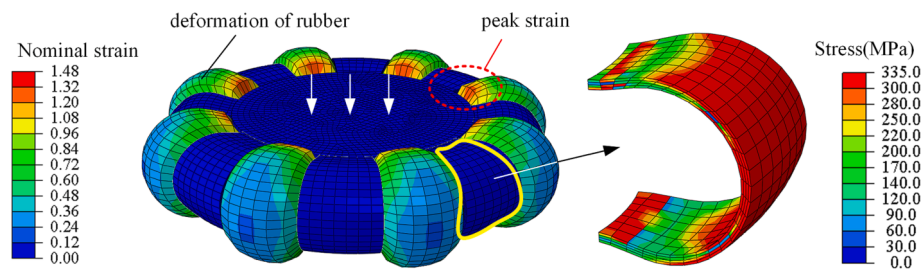


Fig. 15. The SCRB under the vertical load of 330 kN.

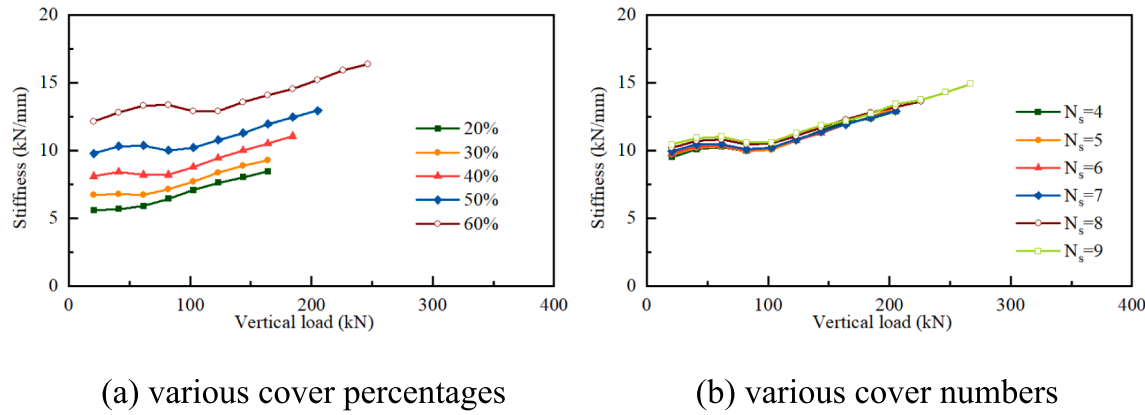


Fig. 16. The vertical stiffness of the SCRB with various steel covers.

steel covers enable the bearing to dissipate energy in the vertical direction. With the hysteresis curve in the vertical direction, the equivalent damping ratio ξ_{eq} can be derived as:

$$\xi_{eq} = \frac{2\Delta W}{\pi(F_1 - F_2)(X_1 - X_2)} \quad (4)$$

where F_1 and F_2 are the maximum and minimum reaction forces at X_1 and X_2 , while ΔW is the energy dissipated in a single loop. As shown in Fig. 18, when the vertical load is small, the equivalent damping ξ_{eq} approximates 0, as the steel covers remain in elastic ranges. With the increase in vertical loads, ξ_{eq} increases as the steel cover dissipation considerable energies. Meanwhile, when the vertical load reaches 180kN, as indicated in Eq. (4), the increase in ΔW is not as large as that in F_1 , so ξ_{eq} stops increasing, even slightly decreases. In summary, the SCRB shows significant damping effects when the vertical load is large.

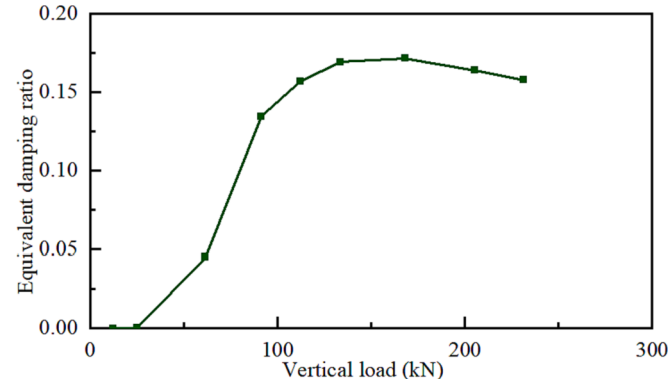


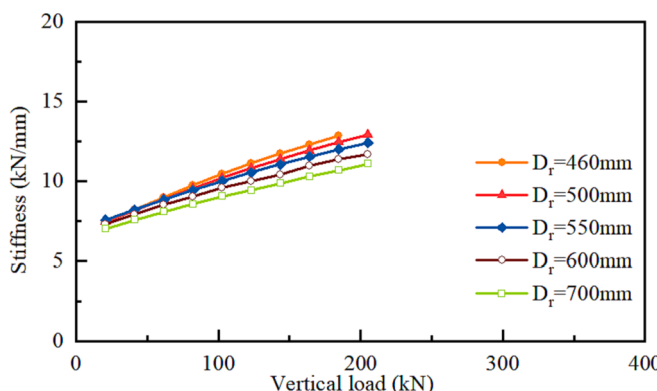
Fig. 18. The equivalent vertical damping ratio of the SCRB under various vertical loads.

3.3. Horizontal behaviors

The steel covers successfully improve the vertical reaction force by the constraining effect, while the vertical stiffness of the SCRB is still small. Meanwhile, to protect the structures from horizontal seismic loads, the SCRB still needs small horizontal stiffness, as well as enough energy dissipation capacity. Therefore, the bearing is loaded horizontally, first with no vertical loads.

Fig. 19 shows the reaction force of the SCRB under continuously increasing horizontal motions up to 50 mm. At the initial stage, the reaction force increases sharply, as the steel covers remain in elastic ranges. After the yield of steel covers, the horizontal stiffness of the SCRB decreases. Different from that in Fig. 4, the steel covers share most of the horizontal force, while the constrain effect has little effect. Therefore, the reaction force of the SCRB can be approximated by the sum of the reaction force of the steel covers and the rubber part.

Fig. 20 shows the strain and stress responses of the deformed SCRB

Fig. 17. The vertical stiffness of the SCRB with various out diameter D_r .

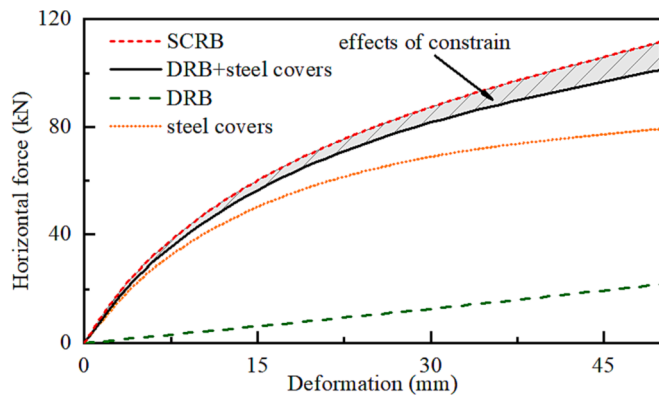


Fig. 19. The reaction force of the SCRB under horizontal motions.

with a horizontal motion of 50 mm. The peak nominal strain, peaking at 37%, occurs at the bulge between steel covers, similar to the strain distribution under vertical loads. The steel covers experience significant plasticity and out-of-plane wrap under the horizontal motion. The plasticity of steel covers starts at terminals, then expands to the midspan.

The steel covers experience significant plastic deformation, which indicates a promising energy dissipation capacity of this bearing. Fig. 21 shows the hysteresis curves of the SCRB under cyclic horizontal motions under various vertical preloads. The SCRB exhibits significant energy dissipation capacity in the horizontal direction, and the estimated equivalent damping ratio is 8.7% at the motion of 20 mm. The increase in the vertical load seems to have little effect on the hysteresis curves of the SCRB, only slightly decreasing the equivalent stiffness K_h , which can be estimated as:

$$K_{eq} = \frac{(F_1 - F_2)}{(X_1 - X_2)} \quad (5)$$

where F_1 and F_2 are the maximum and minimum reaction forces at X_1 and X_2 of a single loop.

As the energy dissipation capacity of the SCRB primarily contributes from the plasticity of the steel, the configuration of steel covers has a significant influence on the SCRB. As shown in Fig. 22(a), the increase in cover percentage significantly improves the energy dissipation capacity of the SCRB, while the SCRB with 40% and 50% cover percentage have similar equivalent damping ratios ξ_{eq} , as the horizontal stiffness also increases.

When the cover percentage keeps unchanged, fewer steel covers result in a larger single curved steel cover, which helps to increase the horizontal stiffness and improve the energy dissipation capacity. As shown in Fig. 22(b), as the cover percentage keeps at 50%, 4 steel covers, instead of the 6-ones configuration, slightly increase ξ_{eq} from 8.4% to 9.5%. The advantages of the smaller N_s configuration contribute

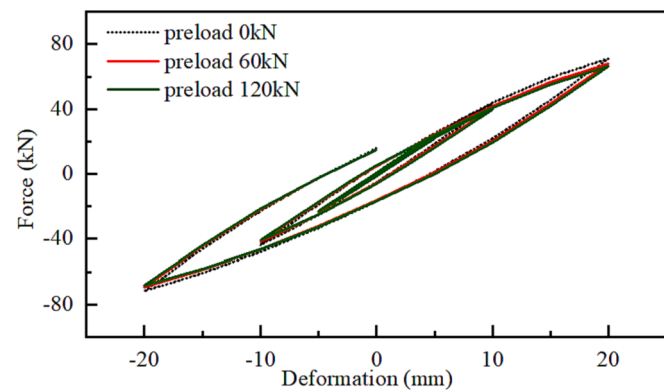


Fig. 21. Hysteresis curves of the SCRB under various vertical preload.

from the curved shape of steel covers, the geometric nonlinearity increases both the stiffness and plastic areas.

Alternatively, the strength of steel covers can be increased by using thicker steel plates. As shown in Fig. 22(c), the increase in the thickness of steel covers significantly increases ξ_{eq} . When t_v reaches 9 mm, ξ_{eq} is up to 17.9%. Meanwhile, the increase in ξ_{eq} also leads to a larger initial horizontal stiffness and yield strength.

The properties of the rubber part also contribute to the mechanical behavior of the SCRB. A large D_r results in a U-shape steel cover instead of a C-shape one, so the horizontal deformation of the SCRB cannot effectively deform flexible steel covers. As shown in Fig. 23, when the outer diameter D_r increases from 430 to 500 mm, the horizontal stiffness and ξ_{eq} decrease significantly. In Contrast, when D_r decreases to only 400 mm, steel covers are approximately C-shaped ones, and the horizontal stiffness of the SCRB is almost the same as the one with D_r of 430 mm. Meanwhile, the C-shaped steel covers improve the energy dissipation capacity of the SCRB, leading to the increase of ξ_{eq} from 7.0% to 13.0% when D_r decreases from 430 to 400 mm.

In summary, the external steel covers prevent the lateral deformation of the rubber part of the SCRB, improving the vertical loading capacity, and the SCRB remains a small vertical stiffness. In addition, SCRB can provide effective damping dissipation when subject to horizontal seismic loads.

4. Design method and effectiveness of the SCRB

4.1. Design method of the SCRB based on the stiffness

The key feature of the SCRB is the small stiffness in both horizontal and vertical directions, so the estimation of the stiffness is the key step in the design of an SCRB. As stated in the previous section, the steel covers constrain the drum-type rubber when the SCRB is subjected to vertical

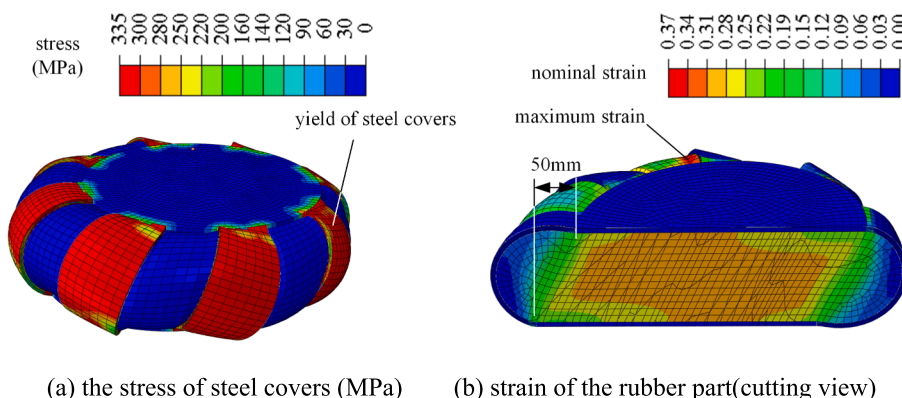


Fig. 20. Strain and stress responses of the SCRB under horizontal motions of 50 mm.

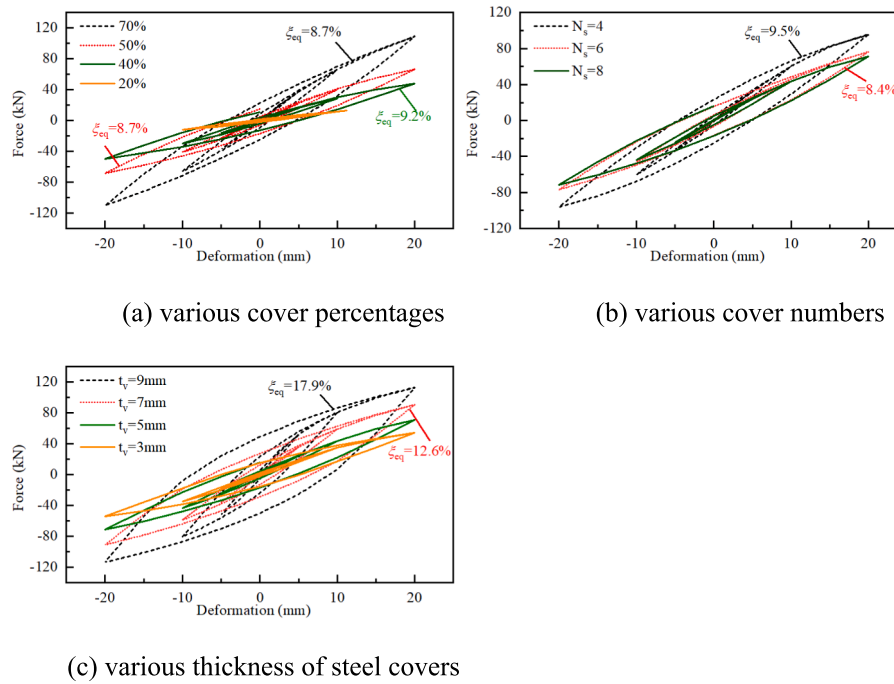


Fig. 22. Hysteresis curves of the SCRB under various steel covers.

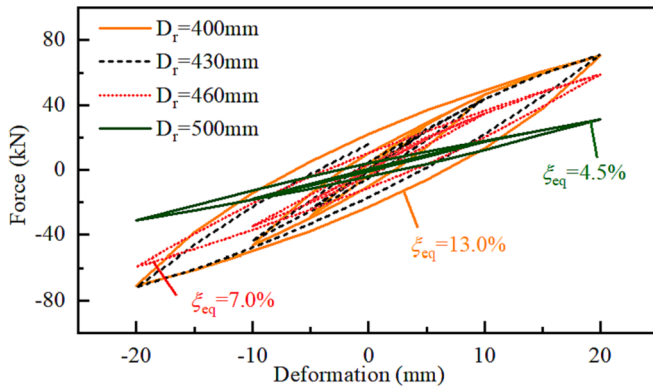


Fig. 23. Hysteresis curves of the SCRB under various diameters.

loads, and the steel covers exhibit complex deformation, like warpage and torsion motions, when there is a horizontal load. Since it is still difficult to estimate the stiffness of the SCRB theoretically, a parametric analysis of the SCRB considering the primary design parameters is performed. Since the mechanical behaviors of the SCRB are complex, the following analysis and design only consider the initial stiffness of the SCRB.

The primary design parameters of the SCRB contain the diameter D_p , the height of the rubber H_r , and the cover percentage S_c . The above analysis shows that the number of the steel cover has little effect on the behaviors when the cover percentage is fixed, so N_s keeps at 8. Further, the height to diameter ratio R_H is introduced to represent the shape of the rubber, as R_H determines the horizontal stiffness of a laminated rubber bearing. The ranges of the primary design parameters are listed in Table 4, the FE models of the SCRB are automatically established using a Python script and the parameters.

The models were loaded vertically and horizontally to obtain the initial stiffness of the SCRB. The results show that the above parameter ranges can result in a vertical stiffness from 3.5 to 52.6 kN/mm and a horizontal stiffness from 1.1 to 27.3 kN/mm. Therefore, part of the SCRB can be used in the isolation for industrial equipment, like electrical

equipment.

In the horizontal direction, as stated in Fig. 19, the reaction force is approximately the sum of that of the drum-type rubber and the steel covers individually. According to the FE results and theoretical formulas, the horizontal stiffness K_H of the SCRB and the drum-type rubber are:

$$K_H = K_{H,\text{steel}} + K_{H,\text{rubber}} = K_{H,\text{steel}} + \frac{G\pi D_p^2}{4H_r} \quad (6)$$

where $K_{H,\text{steel}}$ and $K_{H,\text{rubber}}$ are the horizontal stiffness of the steel covers and the drum-type rubber. As there are 8 steel covers, when the SCRB moves horizontally, some of the steel covers bend and the others torque, making the estimation of the horizontal stiffness quite difficult. Therefore, the influence of the three primary parameters is evaluated, then fitted based on many analyses, to estimate their contributions.

As shown in Fig. 24(a), K_H is proportional to the inverse square of R_H . Further, the coefficient α_{H0} is proportional to the 1.6th power of S_c . The above two numbers of power consider the bending and torsional deformation of the 8 steel covers. Meanwhile, K_H decreases linearly with D_p , as R_H is fixed and the thickness of rubber increases with D_p . The coefficient α_{H3} accounts for the contribution of the steel covers, as when D_p is 0, there are only steel covers in the model.

In the vertical direction, as there is significant interaction between the drum-type rubber and steel covers, the stiffness of the two part cannot be separated apart. As shown in Fig. 25, K_V is also proportional to the inverse square of R_H . Meanwhile, K_V follows a square law of S_c , as steel covers only bend when the SCRB is subjected to vertical loads. Besides, there is a coefficient α_{V2} to account for the contribution of the drum-type rubber. Similar to that in the horizontal direction, K_V increases linearly with D_p , with a coefficient α_{V4} to represent the influence

Table 4
Ranges of the primary design parameters of the SCRB.

Parameter	Range	Reason
D_p (mm)	300 to 800, increase by 50	typical column sizes
R_H	0.2 to 0.5, increase by 0.05	typical R_H of a rubber bearing
S_c	0.2 to 0.6, increase by 0.05	typical cover percentages

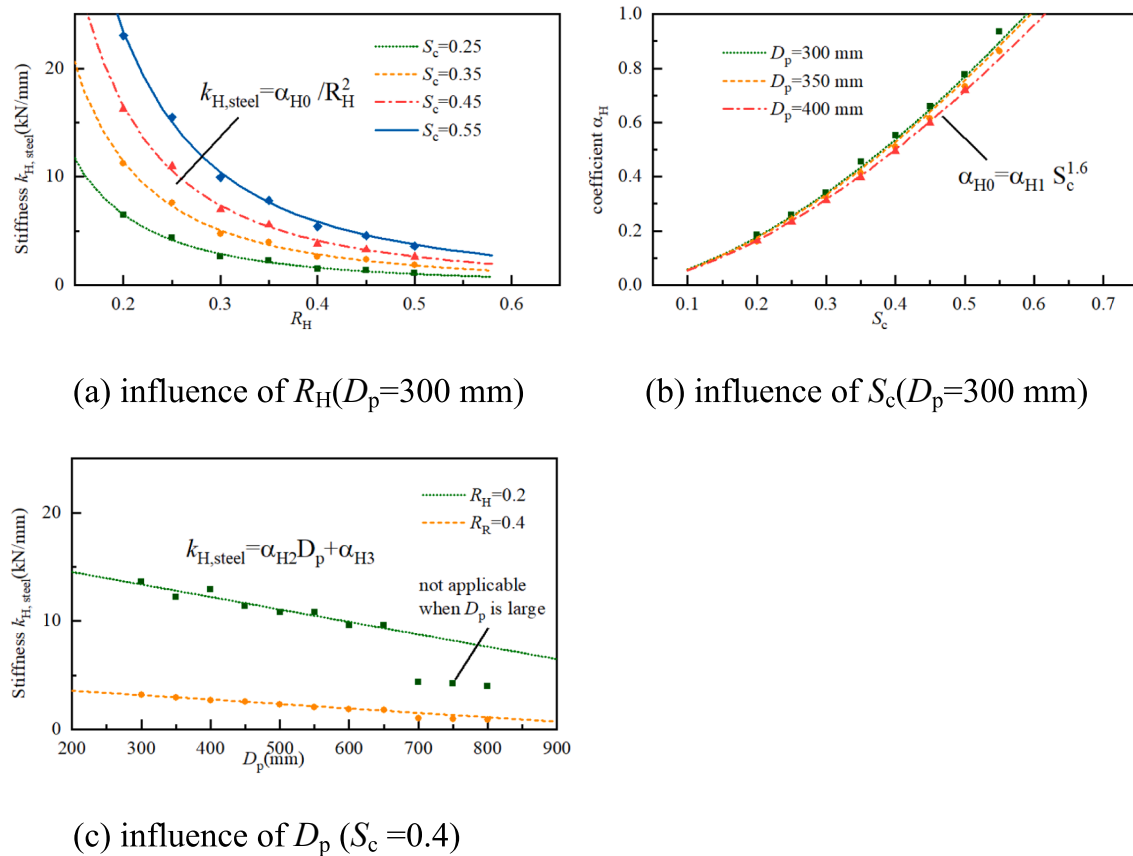


Fig. 24. Influence of the three primary design parameters on the horizontal stiffness $K_{H, \text{steel}}$ of steel covers of the SCRB.

of steel covers.

Based on the above results, the SCRB can be designed following the procedure in Fig. 26. Based on the size of the column, the diameter of the SCRB is preliminarily determined. Then, S_c and R_H are preliminarily selected, and the horizontal and vertical stiffness is estimated. If K_H and K_V cannot satisfy the requirement, S_c and R_H can be adjusted to improve the compatibility of the stiffness. Further, if the adjustment of S_c and R_H still cannot achieve the target, the diameter D_p can be changed, and the workflow continues. Finally, when the parameters result in a satisfactory stiffness, the mechanical behaviors of the SCRB is double checked and further analyzed using the FE model.

4.2. Effectiveness of the SCRB on seismic isolation

The above sections illustrate that the SCRB has a small horizontal and vertical stiffness with considerable energy dissipation capacity. To validate the effectiveness of the SCRB as a three-dimensional isolator, a single-degree-of-freedom (SDOF) system with the SCRB was introduced, as shown in Fig. 27.

The simplified SDOF system is based on a building with many SCRBs. The superstructure is idealized as an SDOF system, with a mass of m_0 and stiffness of k_0 . The SCRB is also idealized as a nonlinear spring, whose constitutional law employs the modified Bouc-Wen model in Table 3. Particularly, two models, namely the vertical and horizontal models, are established to estimate the effectiveness of the SCRB in the vertical and horizontal direction, respectively.

To reduce the computational cost, only one SCRB is included in the model, and the gravity force of m_0 is specified at 245.31 kN. To investigate the effect of the SCRB on various structures, the stiffness k_0 is rewritten as:

$$k_0 = m_0(2\pi f_0)^2 \quad (7)$$

where f_0 is the natural frequency of the superstructure in the horizontal or vertical direction, and f_0 ranges between 0.5 and 10 Hz. To show the effectiveness of the SCRB, we input two seismic records, including the widely-used El Centro record and an artificial record (AW). The PGA is specified at 0.4 g in both the horizontal and vertical directions. The analysis is performed using the central differential method and Python, the time interval is 10^{-3} s.

Fig. 28 shows the peak acceleration response of the fixed and isolated SDOF system under horizontal and vertical excitations. The SCRB can effectively reduce the acceleration response of an SDOF system with a high natural frequency, but has little effect when the superstructure has a low-frequency f_0 . Particularly, the frequency range that makes the effectiveness of the SCRB significant is higher in the vertical direction, as the vertical stiffness of the SCRB is larger than the horizontal one. Generally, a building has much higher eigenfrequencies in the vertical direction than those in the horizontal direction, while the SCRB shows significant effectiveness when f_0 is larger than 6 Hz. Therefore, the SCRB can considerably reduce the vertical and horizontal response of the superstructure.

5. Summary and conclusions

The mechanical behavior and characteristics of SCRB in horizontal and vertical directions are investigated by establishing a detailed FE model and a test on a specimen. The test results validate the correctness of the FE modeling. According to FE analysis and experimental tests, the SCRB resists vertical and horizontal loads through the collaboration of steel covers and rubber.

When the SCRB is subjected to vertical loads, the external steel cover effectively limits the lateral deformation of the rubber, improving the overall stability of the bearing. The parametric analysis of the FE model reveals that the ratio of the steel-covered area has a significant effect on

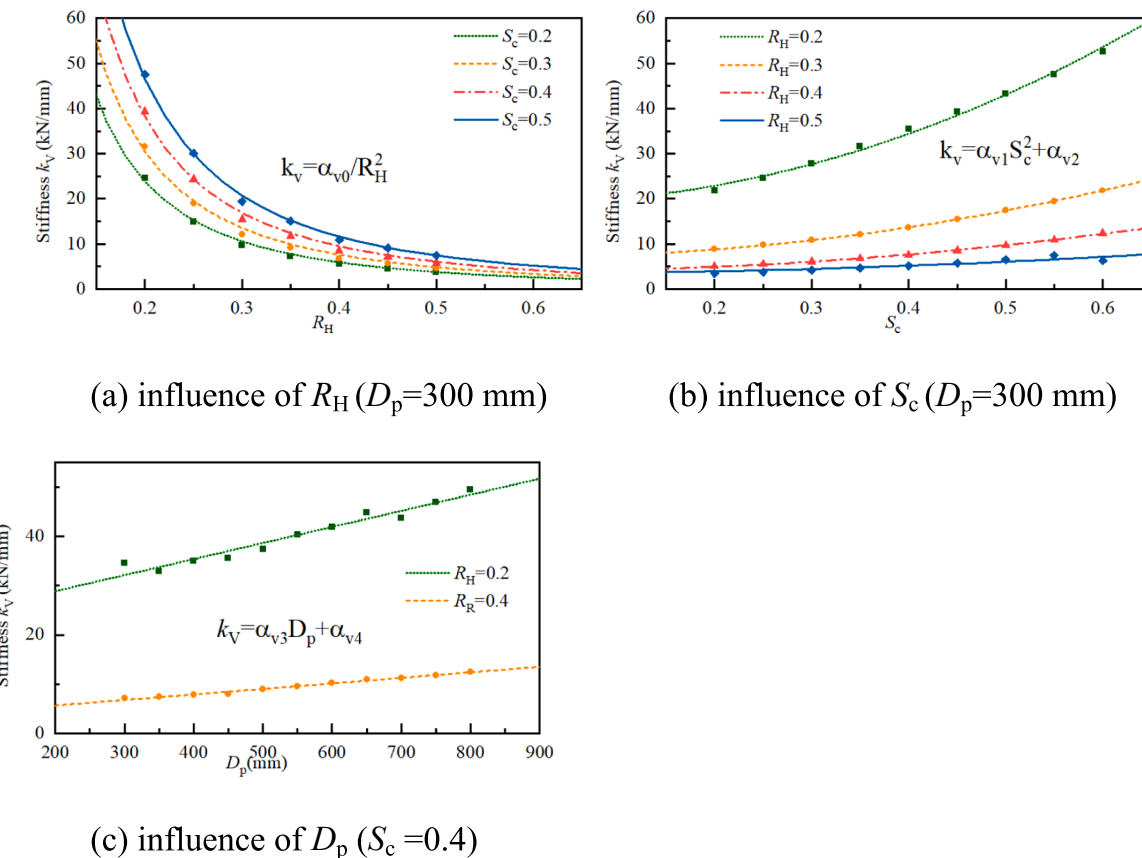


Fig. 25. Influence of the three primary design parameters on the horizontal stiffness of the SCRB.

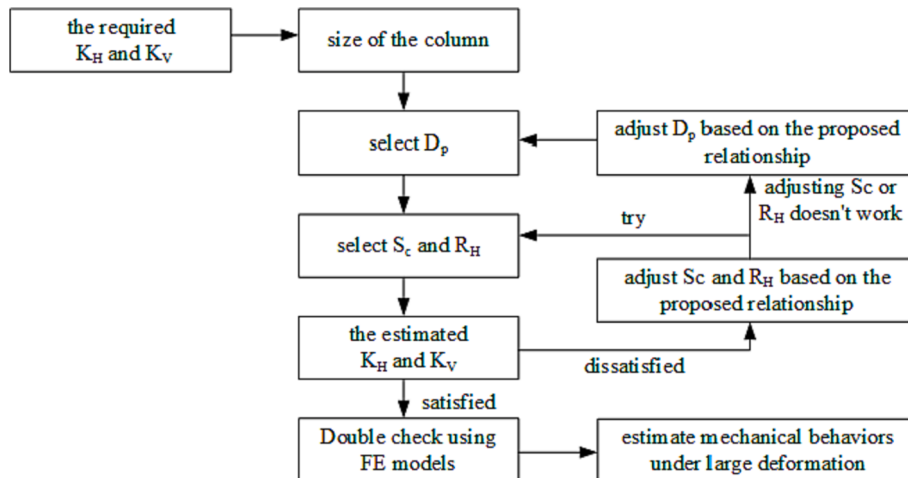


Fig. 26. Design procedure of the SCRB based on the stiffness.

the vertical stiffness of the SCRB. The number of steel covers has little effect on the vertical stiffness, but affects the maximum tensile strain of the rubber. Meanwhile, the vertical stiffness of SCRB is proportional to the inverse square of R_H and the 1.6th power of S_c , decreases linearly with D_p . In addition, the SCRB exhibits significant energy dissipation capability in the vertical direction due to the action of the rubber with the steel cover under vertical load.

Similar to the conventional laminated rubber isolation bearing, SCRB has low horizontal stiffness. At the same time, the external steel cover of SCRB can provide additional horizontal energy dissipation capability. For example, the equivalent damping ratio in the test bearing reaches

30%. The parametric analysis of the FE model shows that the increase in the area coverage of the steel cover leads to larger horizontal stiffness, while has little effect on the equivalent damping ratio. The thickness and length of the bushings have a significant effect on the horizontal stiffness and damping ratio of the bearing. Besides, the horizontal stiffness of SCRB is proportional to the inverse square of R_H and the square of S_c , increases linearly with D_p .

For practical engineering applications, the horizontal and vertical mechanical behaviors of SCRB are simulated using the modified Bouc-Wen model. The mechanical behavior of the SCRB can be accurately described by the modified Bouc-Wen model, which will facilitate the use

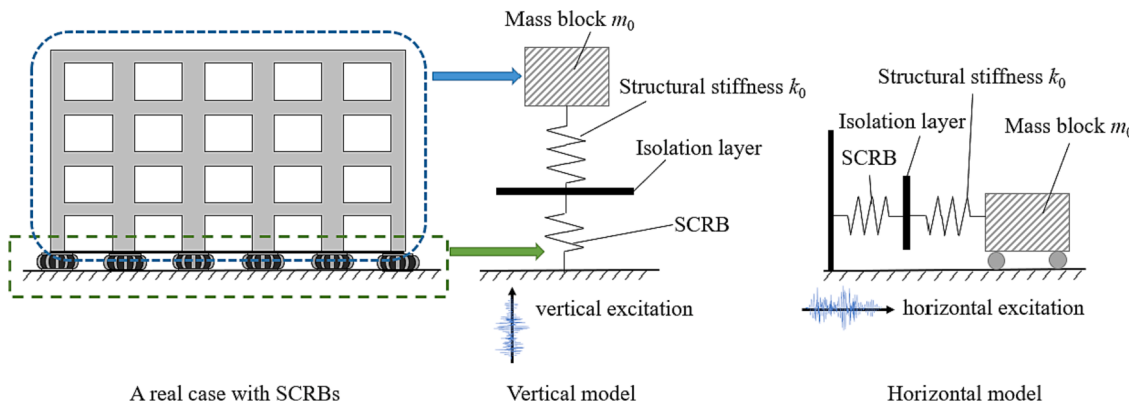


Fig. 27. The simplified model of a building installed on SCRBs.

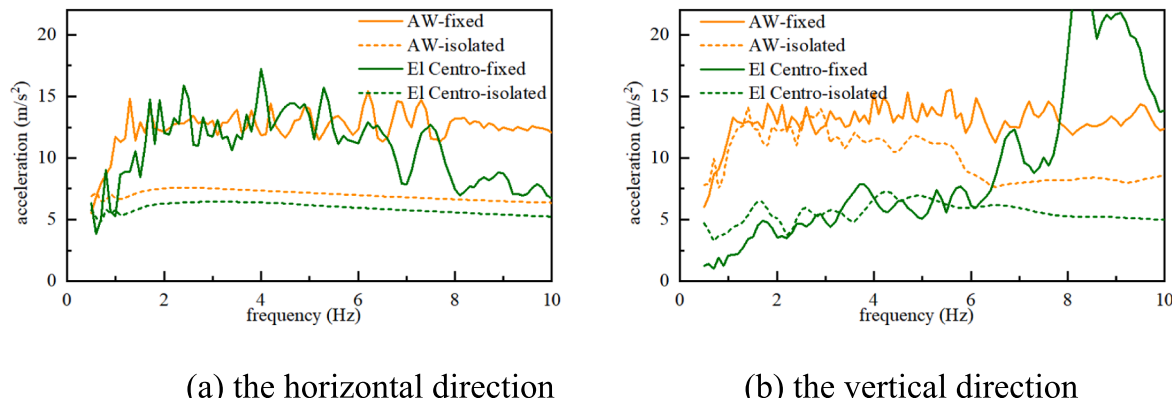


Fig. 28. The peak acceleration response of the SDOF with various natural frequencies.

of the SCRB in practical engineering. Further, based on an SDOF model, the SCRB shows significant effectiveness in reducing the acceleration response of the superstructure under seismic inputs, particularly when the SDOF has a high frequency. The design procedure of the SCRB based on the stiffness is also proposed based on an iteration of parameters.

CRediT authorship contribution statement

Di Wu: Data curation, Resources, Writing – original draft, Funding acquisition. **Yan Xiong:** Conceptualization, Writing – review & editing. **Zhenyu Yang:** Supervision, Methodology, Software, Writing – review & editing.

Declaration of Competing Interest

The authors declare that they have no known competing financial interests or personal relationships that could have appeared to influence the work reported in this paper.

Data availability

Data will be made available on request.

Acknowledgements

The authors are thankful for the support from Science and Technology Planning Project of Guangdong Province (2018B02028003), National Natural Science Foundation of China (52178281, 51778160), Science and Technology Program of Guangzhou, China (201831826).

References

- [1] F. Zhou, P. Tan, Recent progress and application on seismic isolation energy dissipation and control for structures in China, *Earthquake Eng. Eng. Vibr.* 17 (1) (2018) 19–27.
- [2] S. Nagarajaiah, S. Xiaohong, Response of base-isolated USC hospital building in Northridge earthquake, *J. Struct. Eng.* 126 (10) (2000) 1177–1186.
- [3] K. Kasai, A. Mita, H. Kitamura, et al., Performance of seismic protection technologies during the 2011 Tohoku-Oki earthquake, *Earthquake Spectra* 29 (2013) 265–293.
- [4] M. Sarrasin, O. Moroni, C. Neira, et al., Performance of bridges with seismic isolation bearings during the Maule earthquake, Chile, *Soil Dyn. Earthquake Eng.* 47 (2013) 117–131.
- [5] Z. Yang, C. He, Q. Xie, Seismic performance and stiffening strategy of transformer bushings on sidewall cover plates, *J. Constr. Steel Res.* 174 (2020), 106268.
- [6] Y. Yuan, S. Wang, P. Tan, et al., Mechanical performance and shear constitutive model study of a new high-capacity polyurethane elastomeric bearing, *Constr. Build. Mater.* 232 (2020), 117227.
- [7] A. Mordini, A. Strauss, An innovative earthquake isolation system using fibre reinforced rubber bearings, *Eng. Struct.* 30 (10) (2008) 2739–2751.
- [8] W. Wang, X. Wang, A. Li, Coned disc spring compound vertical isolation: testing and modelling, *J. Earthquake Eng.* (2020) 1–33.
- [9] T. Sheng, X. Bian, C. Xiao, et al., Experimental study on a geosynthetics isolator for the base vibration isolation of buildings neighboring metro transportation, *Geotext. Geomembr.* 49 (2021) 1066–1078.
- [10] W. Eltahawy, K.L. Ryan, S. Cesmeci, et al., Parameters affecting dynamics of three-dimensional seismic isolation, *J. Earthquake Eng.* 25 (4) (2021) 730–755.
- [11] W. Eltahawy, K.L. Ryan, Performance of flexible frame building with horizontal and 3D seismic isolation when subjected to 3D ground shaking, *Earthquake Spectra* 36 (4) (2020) 1823–1843.
- [12] Fukasawa T, Okamura S, Yamamoto T, et al. Research and development of thick rubber bearing for SFR. Hysteresis model for thick rubber bearing based on static loading tests. Nippon Kikai Gakkai Ronbunshu (Online), 2018, 84(859): 1700502.1-1700502.20.
- [13] X. Ren, W. Lu, Y. Zhu, et al., Compressive behavior of low shape factor lead-rubber bearings: Full-scale testing and numerical modeling, *Eng. Struct.* 209 (2020), 110030.

- [14] P. Pan, S. Shen, Z. Shen, et al., Experimental investigation on the effectiveness of laminated rubber bearings to isolate metro generated vibration, *Measurement* 122 (2018) 554–562.
- [15] T. Sheng, W. Shi, J. Shan, et al., Base isolation of buildings for subway-induced environmental vibration: Field experiments and a semi-analytical prediction model, *The Structural Design of Tall and Special Buildings* 29 (16) (2020) e1798.
- [16] Zhu X, Lin G, Pan R, et al. Design and analysis of isolation effectiveness for three-dimensional base-seismic isolation of nuclear island building. *Nucl. Eng. Technol.*, 2021 (In Press).
- [17] Z. Chen, Y. Ding, Y. Shi, et al., A vertical isolation device with variable stiffness for long-span spatial structures, *Soil Dyn. Earthquake Eng.* 123 (2019) 543–558.
- [18] Z. Zhou, J. Wong, S. Mahin, Potentiality of using vertical and three-dimensional isolation systems in nuclear structures, *Nucl. Eng. Technol.* 48 (5) (2016) 1237–1251.
- [19] J. Suhara, T. Tamura, Y. Okada, et al., Development of three dimensional seismic isolation device with laminated rubber bearing and rolling seal type air spring, *ASME Pressure Vessels and Piping Conference* 46563 (2002) 43–48.
- [20] M.M. Pourmasoud, J.B.P. Lim, I. Hajirasouliha, et al., Multi-directional base isolation system for coupled horizontal and vertical seismic excitations, *J. Earthquake Eng.* (2020) 1–26.
- [21] K. Faramarz, R. Montazar, Seismic response of double concave friction pendulum base-isolated structures considering vertical component of earthquake, *Adv. Struct. Eng.* 13 (1) (2010) 1–13.
- [22] Q. Han, M. Jing, Y. Lu, et al., Mechanical behaviors of air spring-FPS three-dimensional isolation bearing and isolation performance analysis, *Soil Dyn. Earthquake Eng.* 149 (2021), 106872.
- [23] W. Xie, Y. Du, L. Sun, et al., Study on the Stiffness Correction Method of Novel Antivibration Bearing for Urban Rail Transit Viaduct, *Shock Vib.* 2017 (2017).
- [24] W. Liu, H. Xu, W. He, et al., Static test and seismic dynamic response of an innovative 3D seismic isolation system, *J. Struct. Eng.* 144 (12) (2018) 04018212.
- [25] T. Li, Q. Su, S. Kaewunruen, Seismic metamaterial barriers for ground vibration mitigation in railways considering the train-track-soil dynamic interactions, *Constr. Build. Mater.* 260 (2020), 119936.
- [26] S. Diego, J.A. Casado, I. Carrascal, et al., Numerical and experimental characterization of the mechanical behavior of a new recycled elastomer for vibration isolation in railway applications, *Constr. Build. Mater.* 134 (2017) 18–31.
- [27] R. Zakeri, S.N.M. Tafreshi, A.R. Dawson, et al., Influence of rubber sheet on dynamic response of machine foundations, *Constr. Build. Mater.* 274 (2021), 121788.
- [28] H. Li, S. Tian, X. Dang, et al., Performance of steel mesh reinforced elastomeric isolation bearing: Experimental study, *Constr. Build. Mater.* 121 (2016) 60–68.
- [29] P.M. Osgooei, M.J. Tait, D. Konstantinidis, Three-dimensional finite element analysis of circular fiber-reinforced elastomeric bearings under compression, *Compos. Struct.* 108 (2014) 191–204.
- [30] W. Yang, X. Sun, M. Wang, et al., Vertical stiffness degradation of laminated rubber bearings under lateral deformation, *Constr. Build. Mater.* 152 (2017) 310–318.
- [31] A.R. Bhuiyan, E. Ahmed, Analytical expression for evaluating stress-deformation response of rubber layers under combined action of compression and shear, *Constr. Build. Mater.* 21 (9) (2007) 1860–1868.
- [32] Y. Wu, H. Wang, A. Li, et al., Explicit finite element analysis and experimental verification of a sliding lead rubber bearing, *J. Zhejiang Univ.-SCIENCE A* 18 (5) (2017) 363–376.
- [33] J. Yoshida, M. Abe, Y. Fujino, et al., Three-dimensional finite-element analysis of high damping rubber bearings, *J. Eng. Mech.* 130 (5) (2004) 607–620.
- [34] J. Sheikhi, M. Fathi, R. Rahnavard, et al., Numerical analysis of natural rubber bearing equipped with steel and shape memory alloys dampers, *Structures* 32 (2021) 1839–1855.
- [35] M. Saadatnia, H.T. Riahi, M. Izadinia, Hysteretic Behavior of Rubber Bearing With Yielding Shear Devices, *Int. J. Steel Struct.* 19 (3) (2019) 747–759.
- [36] H. Kakolvand, M. Ghazi, B. Mehrparvar, et al., Experimental and numerical study of a new proposed seismic isolator using steel rings (SISR), *J. Earthquake Eng.* (2020) 1–30.
- [37] Wu D, Xiong Y, Cui J. Three-dimensional seismic isolation bearing with anti-extraction, China Patent, CN210117820U.2020 Feb 28.
- [38] General Administration of Quality Supervision, Inspection and Quarantine of China. Rubber bearing-part 3: Elastomeric seismic-protection isolators for buildings, GB 20688.3-2006.2006.
- [39] B.Y. Moon, G.J. Kang, B.S. Kang, et al., Design and manufacturing of fiber reinforced elastomeric isolator for seismic isolation, *J. Mater. Process. Technol.* 130 (2002) 145–150.
- [40] F. Paolacci, R. Giannini, Study of the effectiveness of steel cable dampers for the seismic protection of electrical equipment, in: Proceedings of 14th World Conference on Earthquake Engineering, 2008, pp. 12–17.
- [41] Z. Yang, Q. Xie, C. He, et al., Numerical investigation of the seismic response of a UHV composite bypass switch retrofitted with wire rope isolators, *Earthq. Eng. Vibr.* 20 (1) (2021) 275–290.